Chinese Chemical Letters 34 (2023) 107792

Contents lists available at ScienceDirect

Chinese Chemical Letters

journal homepage: www.elsevier.com/locate/cclet

Structure-property relationship on aggregation-induced emission properties of simple azine-based AIEgens and its application in metal ions detection

Xiao-Mei Sun[a], Juan Liu[b], Zhao-Hui Li[c], Yong-Peng Fu[d], Ting-Ting Huang[a], Zhong-Di Tang[a], Bingbing Shi[a], Hong Yao[a], Tai-Bao Wei[a], Qi Lin[a,*]

[a] College of Chemistry and Chemical Engineering, Northwest Normal University, Lanzhou 730070, China
[b] Key Laboratory of Environment-Friendly Composite Materials of the State Ethnic Affairs Commission, College of Chemical Engineering, Northwest Minzu University, Lanzhou 730000 China
[c] Department of Pharmacy Jiangxi Medical College, Shangrao 334000, China
[d] Longnan Ecological and Environmental Monitoring Centre of Gansu Province, Longnan 746000, China

ARTICLE INFO

Article history:
Received 9 June 2022
Revised 27 August 2022
Accepted 29 August 2022
Available online 31 August 2022

Keywords:
AIEgens
Structure-property relationship
Fluorescent chemosensor
Azine derivatives
Calculations

ABSTRACT

In recent twenty years, aggregation-induced emission (AIE), due to its excellent application prospect, has aroused widespread interests. The development of novel and easy to make AIE luminogens (AIEgens) is an attractive subject. For this purpose, it is very important to study the structure-property relationship of AIEgens. Because azine derivatives are easy to synthesis and some of them have nice AIE properties, herein, a series of azine derivatives (**ADs**) were employed as models to study the influence of different functional groups, electronic effects and structures on the AIE properties of azine derivatives. The AIE mechanism were studied by single crystal analysis, density functional theory (DFT) calculations and so on. The results indicated that the *o*-hydroxyl aryl substituted azine compounds could show good AIE properties. Meanwhile, the AIE properties of *o*-hydroxyl aryl substituted azine compounds were also influenced by the electronic effects of the aryl groups in the azine compounds. The *o*-hydroxyl groups could form intramolecular hydrogen bond with imine group, which play key role to restrict the intramolecular rotation of the aryl groups and act as base stone for the AIE process of this kind compounds. The HOMO-LUMO energy gaps of *o*-hydroxyl substituted azine are smaller than other homologous compounds, which is agree with the proposed AIE mechanism. Finally, thanks to the AIE properties, the *o*-hydroxy-substituted azines could be used as efficient Al^{3+} and Cu^{2+} fluorescent chemosensors in different conditions. In addition, test strips based on **AD10** has been prepared, which can conveniently detect Cu^{2+} in industrial wastewater. This research supplied a way for the design of novel easy to make AIEgens through simple azine derivatives.

In recent two decades, aggregation induced emission (AIE) [1] has received more and more attention in many fields due to its unique properties and wide range of applications. It provides an excellent platform for the development of useful luminescent materials [2]. At the same time, due to its unique luminescence behavior and strong aggregation state fluorescence emission, AIE has shown a wide range of applications in fluorescence sensors [3], organic light-emitting diodes (OLED) [1,4], biological imaging [1] and functional materials [5]. So far, many AIEgens with adjustable color and high quantum yield have been reported such as hexaphenylsilole [6], tetraphenylethylene [7], and so on [8–10]. Although there are various AIEgens had been reported, the development of simple, high efficiency and easy to synthesis AIEgen is always an attractive task. While, we all know that the structure of AIEgens plays an important role in the AIE properties. Therefore, it is very important to deeply understand the AIE mechanism and structure-property relationship of AIEgens, which very helpful to design efficiency AIEgens.

Azine derivatives are easy to synthesize [11] and some of them have good AIE properties and can be used in chemical sensors [12] and biological imaging [13]. Moreover, Azine derivatives with different structure showed different AIE properties [14,15]. Therefore, systematic study of AIE mechanism and structure-property relationship [16,17] of these compounds can help us deeply under-

* Corresponding author.
E-mail address: linqi2004@126.com (Q. Lin).

https://doi.org/10.1016/j.cclet.2022.107792
1001-8417/

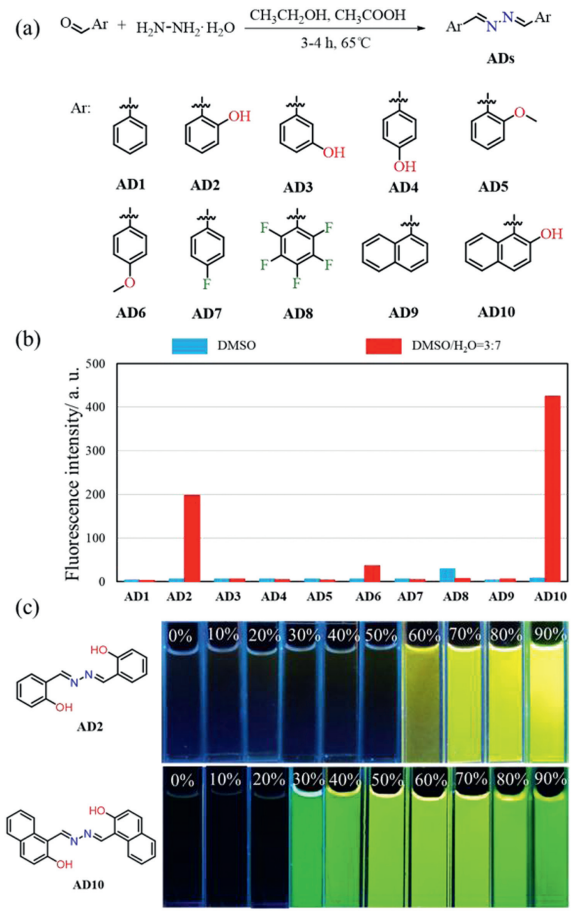

Fig. 1. (a) The synthetic route of **ADs**. (b) Fluorescence intensity of **ADs** (1×10^{-5} mol/L, $\lambda_{ex} = 365$ nm, Slit = 5/10 nm) in DMSO and DMSO/H_2O = 3:7 binary solution. (c) Fluorescence photos of **AD2** and **AD10** in DMSO/H_2O binary solution with different volumetric fractions of water.

standing the AIE mechanism of this kind of AIEgens and provide ideas for the design, synthesis and application of new simple and efficient AIEgens.

In view of these, as part of our research interest in AIE-based supramolecular materials, herein, the AIE mechanism and structure-property relationship of simple azine-based AIEgens have been carefully investigated. As shown in Fig. 1a, firstly, a series of azine derivatives **ADs** including **AD1**∼**AD10** which containing various functional substitute groups such as electrondrawing, electron-donor as well as hydrogen bonding groups have been synthesized. Secondly, the AIE mechanism as well as the influence of substitute groups and structure on AIE property of these azine derivatives have been carefully studied by experiments, single crystal structure and theoretical calculations. Interestingly, the *o*-hydroxyl aryl substituted azine compounds **AD2** and **AD10** show good AIE performance, and the *o*-hydroxyl groups play key role to restrict the intramolecular rotation of the aryl groups which induced the AIE. Meanwhile, based on the AIE, the **AD2** and **AD10** can be used to selectively fluorescent detection Al^{3+} and Cu^{2+} in aqueous solution.

In order to study the structure-property relationship of azine derivatives on the performance of AIE, the fluorescence properties of **ADs** were primarily investigated in a series of organic-water (organic solvents are DMSO, acetone or THF) binary solutions with different water contents (Figs. S7-S15 in Supporting information). According to these experiments, as shown in Figs. S7-S15, Figs. 1b and c, with the increasing of the water volume fraction, the fluorescence emission intensity of the **AD2** DMSO-H_2O solution showed a gradual increase at $\lambda_{em} \approx 530$ nm and reached the strongest state when the water volume fraction is 90%. While, in this process, the UV absorption of **AD2** showed gradually decreases (Fig. S16a in Supporting information). The fluorescence quantum yield of **AD2** in DMSO:H_2O = 1:9 was calculated to be 0.27 (Figs. S17 and S18 in Supporting information) [18]. Similarly, the fluorescence emission intensity of **AD10** DMSO-H_2O solution showed a gradual increase at $\lambda_{em} \approx 530$ nm and reached the strongest state when the volume fraction of water is 70%. In this process, the UV absorption of **AD10** showed gradually decreases under the 30%∼60% water volume fractions (Fig. S16b in Supporting information) and slight increase at 70%∼90% water volume fractions. The fluorescence quantum yield of **AD10** in DMSO:H_2O = 3:7 was calculated to be 0.77 (Figs. S17 and S19 in Supporting information) [18]. These results indicated that **AD2** and **AD10** possess AIE property in DMSO-H_2O solution. While, in acetone-H_2O or THF-H_2O system, the **AD2** and **AD10** also have similar AIE property (Figs. S7-S15). However, according to Figs. S7-S15, other eight compounds **AD1** and **AD3**∼**AD9** have no obvious AIE properties in these organic-water systems. According to these results, we can find that the *o*-hydroxyl aryl substituted azine compounds **AD2** and **AD10** show good AIE performance, and the *o*-hydroxyl aryl groups play key role in the AIE process.

Secondly, it is noteworthy that the HOMO-LUMO gap of **AD9** is smaller than that of **AD2**, but **AD9** does not exhibit AIE properties. Among **AD1**∼**AD10**, **AD2** and **AD10** are *o*-hydroxyl ary substituted azines (Figs. 2a and b). This result indicated that the *o*-hydroxyl substituting for aryl group in the azine is the key factor for the AIE of this kind of compounds. The single crystal structure and theoretical calculations can help us better understand the role of *o*-hydroxyl group in the AIE properties of the azines. As shown in Fig. 2e, the *o*-hydroxyl group could form intramolecular hydrogen bonds, which could restrict the intramolecular rotation of the aryl groups, this is the foundation of the AIE for **AD2** and **AD10**. Meanwhile, according to theoretical calculations, as shown in Fig. 2c and Fig. S21 (Supporting information), in ESP diagrams of **AD2** and **AD10**, hydroxyl oxygen atoms have a negative charge distribution, and N of C=N unit has a positive charge distribution. Therefore, the *o*-hydroxyl group could conduct unique excited state intramolecular proton transfer (ESIPT) process with C=N group, which also lead **AD2** and **AD10** producing strong AIE properties. While, other **ADs** could not form stable intramolecular hydrogen bonds and could not show AIE property.

In order to gain a deeper understanding of aggregating process of **AD2** and **AD10**, the non-covalent interactions in adjacent **AD2** and **AD10** molecules were carefully investigated by independent gradient model (IGM) and single crystal structure analysis. As shown in Fig. 2d, in the IGM, the strength of the interaction can be characterized by the volume and color of the adjacent **AD2** and **AD10** molecular interaction region, so the green region appears as a weak interaction, such as the formation of the van der Waals interaction. The blue areas indicate strong interactions, such as hydrogen bonds that form. The IGM diagram shows that **AD2** and **AD10** have strong intramolecular hydrogen bonds and there are intermolecular hydrogen bonds, π-π and C-H$\cdots\pi$ interaction existing in adjacent molecules.

Moreover, the single crystal structure analysis also supporting the calculated aggregating process, as shown in Fig. 2e, in the crystal, each **AD2** and **AD10** molecules adopt a completely planar conformation. In addition, there are strong intramolecular hydrogen bonds between the nitrogen atoms of the **AD2** and **AD10** azine units and the *o*-hydroxyl on the aryl groups, and the distances are 1.89 Å and 1.85 Å respectively. The strong intramolecular hydrogen bonds greatly enhance the rigidity of the molecule and contribute to the planarization of the molecule. Meanwhile, as shown

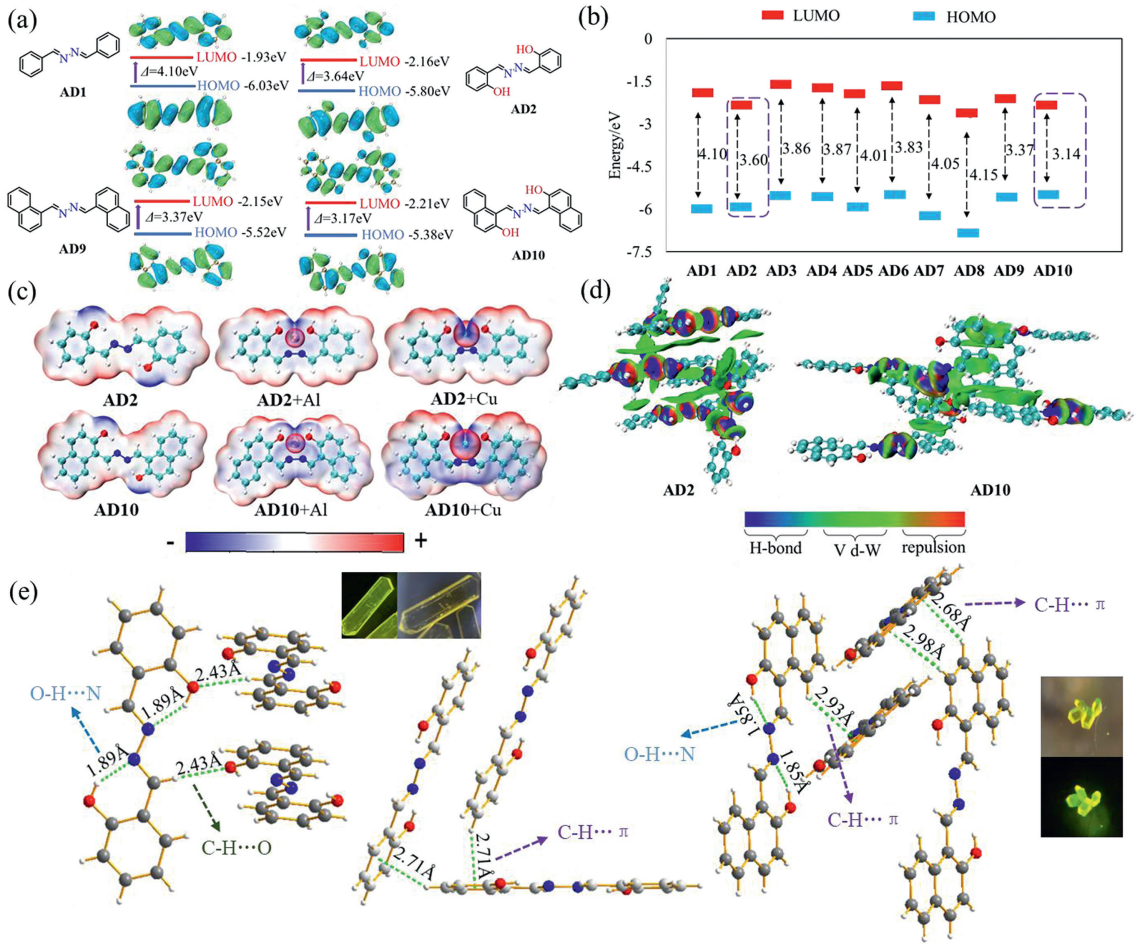

Fig. 2. (a) The HOMO and LUMO orbital gaps of single molecule of **AD1**, **AD2**, **AD9** and **AD10**. (b) The HOMO and LUMO orbital gaps of single molecule of **AD1**~**AD10**. (c) ESP of **AD2**, **AD2**+Al, **AD2**+Cu and **AD10**, **AD10**+Al, **AD10**+Cu. (d) The colored scatter plots isosurfaces of IGM of **AD2** and **AD10**. (e) The various intermolecular interactions in single crystal of **AD2** and **AD10**.

in Fig. 2e, among the adjacent molecules of **AD2**, there are intermolecular C-H···O hydrogen bonds ($d = 2.43$ Å). Moreover, there are several kinds of C-H···π ($d = 2.43$~2.98 Å, Fig. 2e) interactions existing among the adjacent molecules of **AD2** and **AD10**. In addition, several kinds of π-π interactions also exists between ary ring ($d = 4.74$ Å, Fig. S22 in Supporting information) and C=N double bond (d =3.38 Å, Fig. S22) in **AD2**. Furthermore, in **AD10**, the binary ring ($d = 6.11$ Å > 6.0 Å, Fig. S23 in Supporting information), there is no π-π interaction [19], but there is also π-π interaction between naphthalene ring and C=N double bond ($d = 4.28$ Å, Fig. S23). These intramolecular and intermolecular supramolecular interactions including hydrogen bonds, C-H···π and π-π interactions not only lead the aggregate of **AD2** and **AD10** but also restricted the intramolecular rotation and induced the AIE of these two compounds.

In light of the nice AIE properties of **AD2** and **AD10**, the application property of these two AIE compounds have been investigated as metal ions sensor by separately adding 20 equiv. different cations including Mg^{2+}, Ca^{2+}, Cr^{3+}, Fe^{3+}, Co^{2+}, Ni^{2+}, Al^{3+}, Cu^{2+}, Zn^{2+}, Ba^{2+}, Ag^{+}, Cd^{2+}, Hg^{2+}, Pb^{2+}, Tb^{3+}, Eu^{4+} and La^{3+} (aqueous solution, 0.1 mol/L) in to the DMSO/H_2O (v:v = 8:2) solution of **AD2** and **AD10**, respectively. As shown in Fig. 3a and Fig. S27a (Supporting information), the free **AD2** and **AD10** showing very weak fluorescence in DMSO/H_2O (v:v = 8:2) solution, after the addition of Al^{3+}, the fluorescence of **AD2** at $\lambda_{em} \approx 450$ nm and **AD10** at $\lambda_{em} \approx 530$ nm show "turn on" response, and other ions could not lead similar response, which indicated that **AD2** and **AD10** can selectively recognize Al^{3+} through fluorescence "turn on" model in DMSO/H_2O (v:v = 8:2) solution. According to the fluorescence titrations (Fig. 3d and Fig. S27d in Supporting information), the lowest detection limit (LOD) of **AD2** and **AD10** for Al^{3+} recognitions were calculated as 1.94×10^{-7} mol/L and 8.47×10^{-6} mol/L, respectively. Meanwhile, based on the competitive experiments (Fig. 3c and Fig. S27c in Supporting information), other ions could not interfere in Al^{3+} recognition processes. As shown in Fig. S28 (Supporting information), the detection rate also has been investigated, after the Al^{3+} (3×10^{-4} mol/L) was added to **AD10** in (1×10^{-5} mol/L) DMSO:H_2O = 8:2 solution, the fluorescence of the solution increased rapidly and achieved to the maximum after within 50 min.

In addition, as shown in Fig. 3b and Fig. S27, in DMSO/H_2O (v:v = 1:9) and DMSO/H_2O (v:v = 3:7) solutions, **AD2** and **AD10** show good AIE phenomenon, after the addition of Cu^{2+} into these solutions, the AIE fluorescence of **AD2** and **AD10** quenched, and other ions could not induce similar response. Therefore, the **AD2** and **AD10** can selectively recognize Cu^{2+} in DMSO/H_2O (v:v = 1:9) and DMSO/H_2O (v:v = 3:7) solution, respectively. Through fluorescence titrations (Figs. S29-S31 in Supporting information), the LOD of **AD2** and **AD10** for Cu^{2+} were measured as 8.76×10^{-8} mol/L and 1.73×10^{-7} mol/L, respectively. As shown in Fig. S29, other ions could not interfere in the Cu^{2+} sensing process.

In order to further develop the practical application of the **ADs**, test strips based on **AD10** were prepared to detect Cu^{2+}. As shown

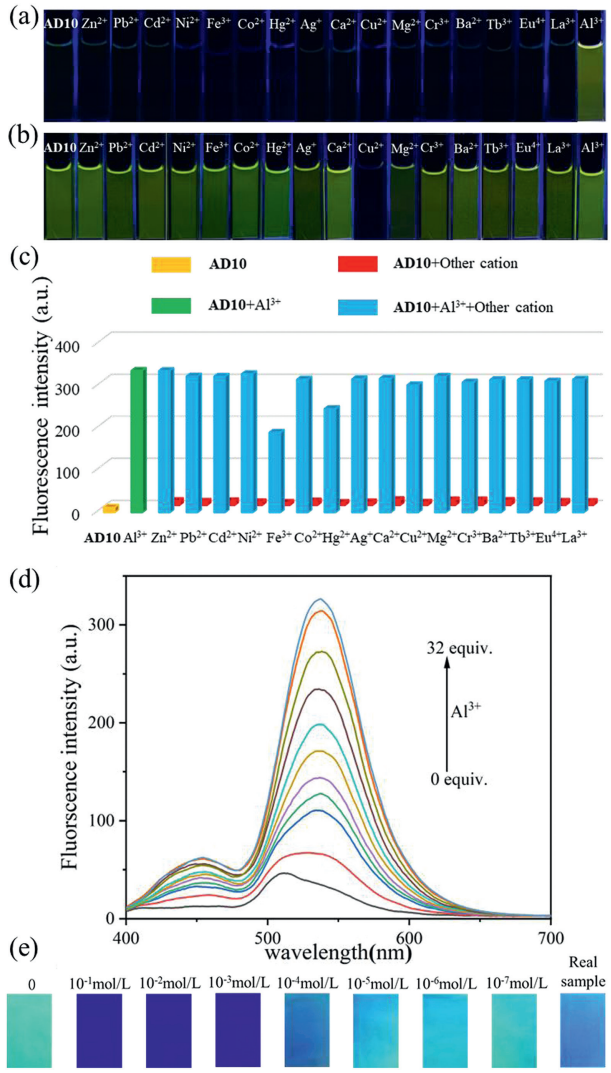

Fig. 3. Fluorescence photo of **AD10** (1×10^{-5} mol/L) in the presence of 20 equiv. of various metal ions in (a) DMSO/H_2O (v/v = 8:2) and (b) DMSO/H_2O (v/v = 3:7) binary solution (λ_{ex} = 365 nm). (c) competitive experiments of the sensor **AD10** (1×10^{-5} mol/L) with addition of 20 equiv. of Al^{3+} and 20 equiv. of other common ions. (d) Fluorescence titrations spectra of **AD10** (1×10^{-5} mol/L) after the addition of 0-32 equiv. of Al^{3+} into the DMSO/H_2O (v/v = 8:2) binary solution. (e) Fluorescence changes of **AD10**-based test strips after the addition of different concentration ($1 \times 10^{-1} \sim 1 \times 10^{-7}$ mol/L) of Cu^{2+}.

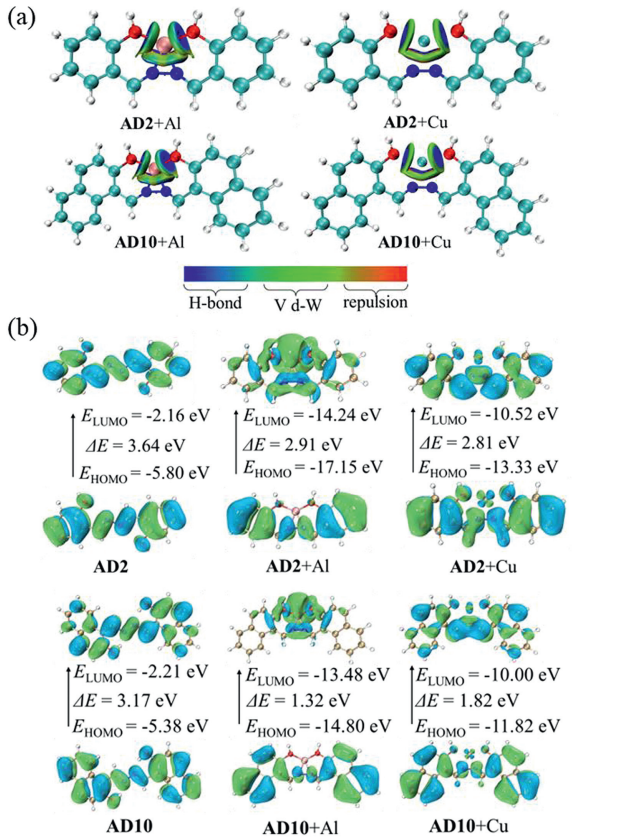

Fig. 4. (a) The colored scatter plots isosurfaces of IGM of **AD2**+Al, **AD2**+Cu, **AD10**+Al and **AD10**+Cu. (b) The HOMO-LUMO of **AD2**, **AD2**+Al, **AD2**+Cu and **AD10**, **AD10**+Al, **AD10**+Cu by DFT optimized.

in Fig. 3e, the test strips could show fluorometric response for different concentrations of Cu^{2+} under a 365 nm UV lump. Interestingly, the test strips could be applied to detect in real sample of Cu^{2+} containing wastewater from the industry.

In order to verify the structure property relationships of the azine derivatives for metal ions recognitions, the similar experiments were carried out on **AD1** and **AD3**∼**AD9**. However, as shown in Figs. S24-S26 (Supporting information), **AD1** and **AD3**∼**AD9** could not show any selective response for metal ions. Therefore, the *o*-hydroxyl substituted aryl groups in **AD2** and **AD10** play important role not only in the AIE but also in ions sensing processes of the azine derivatives.

Additionally, the ^1H NMR, FT-IR and ESI-MS experiments as well as theoretical calculation were applied to investigated the Al^{3+} and Cu^{2+} recognition mechanism of **AD2** and **AD10**. According to the host-guest ^1H NMR spectra (Fig. S32 in Supporting information), after adding Al^{3+}, the proton signals of H_a (-OH) and H_b (CH=N) on **AD2** showed distinct downfield shifts, which could attribute to the Al^{3+} coordinated with O (-OH) and N (CH=N) on **AD2**. Meanwhile, the proton signals of H_c-H_f on benzene groups also showed a slightly downfield shifts (Fig. S32), which could be attributed to the coordination of Al^{3+} with **AD2** induced deshielding effect. Meanwhile, in FT-IR spectra (Fig. S34 in Supporting information), after complexing with Al^{3+}, the stretching vibration peaks of CH=N and -OH on **AD2** change from 1622 cm^{-1}, 3438 cm^{-1} to 1614 cm^{-1}, 3427 cm^{-1}, respectively, which also indicated that Al^{3+} coordinated with O (-OH) and N (CH=N) on **AD2**. This proposed coordination mechanism of **AD2**+Al also supported by theoretical calculation, as shown in Fig. 4a, the IGM diagram shows that **AD2** has strong coordination bonds with Al^{3+}. Meanwhile, after the **AD2** coordinated with Al^{3+}, the HOMO-LUMO gap decreased (Fig. 4b), which also indicated the formation of stable complex. Moreover, in the HR-MS (Fig. S36 in Supporting information), the peak at 329.1076 corresponding to [**AD2**·Al·H_2O·CH_3CH_2OH-2H]$^+$, which revealed a 1:1 complex ratio between **AD2** and Al^{3+}.

Then, the fluorescent response mechanism of the **AD2** for Al^{3+} has been investigated by theoretical calculation [20]. According to the ESP (Fig. 2c) and HOMO-LUMO (Fig. 4b) of **AD2**, with the coordination of **AD2** with Al^{3+}, a clear electron transition from O (-OH) and N (CH=N) on **AD2** to Al^{3+} could be observed. This result revealed that the coordination of Al^{3+} with **AD2** not only restricted the intramolecular rotation of **AD2**, but also caused the photoinduced electron transfer (PET) process of compound **AD2** is forbidden [21], making the fluorescence of the solution "turn on". Similarly, as shown in Figs. 2c and 4a, Figs. S33-S38 (Supporting information), the **AD10** has a similar recognition mechanism for Al^{3+}.

Meanwhile, Cu^{2+} recognition mechanism of **AD2** and **AD10** also has been investigated. In FT-IR spectra (Fig. S34), after complex-

ing with Cu^{2+}, the stretching vibration peaks of CH=N and -OH on **AD2** change from 1622 cm^{-1}, 3438 cm^{-1} to 1592 cm^{-1}, 3422 cm^{-1}, respectively, indicating that Cu^{2+} coordinated with O (-OH) and N (CH=N) on **AD2**. This proposed coordination mechanism of **AD2**+Cu also supportd by theoretical calculation, as shown in Fig. 4a, the IGM diagram shows that **AD2** has strong coordination bonds with Cu^{2+}. Meanwhile, after the **AD2** coordinated with Cu^{2+}, the HOMO-LUMO gap decreased (Fig. 4b), which also indicated the formation of stable complex. Meanwhile, in the HR-MS (Fig. S37), the peak at 302.0226 corresponding to [**AD2**·Cu-H]$^+$, which revealed a 1:1 complex ratio between **AD2** and Cu^{2+} (Fig. 4a).

Then, the fluorescent response mechanism of the **AD2** for Cu^{2+} has been investigated by theoretical calculation. According to the ESP (Fig. 2c) and HOMO-LUMO (Fig. 4b) of **AD2**, with the coordination of **AD2** with Cu^{2+}, a clear electron transition from O (-OH) and N (CH=N) on **AD2** to Cu^{2+} could be observed. The formation of complex will bend the rigid structure of **AD2**, leading to the rearrangement of **AD2**, and strong chelation enhances fluorescence quenching [22]. In addition, the coordination also destroys the OH···N hydrogen bond within the molecule, which seriously interferes with the formation of AIE system. Moreover, the paramagnetic of Cu^{2+} also is a reason for fluorescent quenching [21]. All these factors lead the addition of Cu^{2+} quenching the fluorescence of **AD2**. Similarly, as shown in Fig. 4, Figs. S35-S39 (Supporting information), **AD10** also has a similar Cu^{2+} recognition mechanism.

In this paper, the AIE mechanism and structure-property relationship of simple azine-based AIEgens have been carefully investigated. Because the **AD2** and **AD10** have *ortho*-hydroxyl groups, they can form intramolecular hydrogen bonds and prevent intramolecular rotation, so they show good AIE properties. However, the **AD1** and **AD3**∼**AD9** could not form intramolecular hydrogen bond, therefore they have no AIE properties. In addition, **AD2** and **AD10** can selectively recognize Al^{3+} and Cu^{2+} in different DMSO/H_2O systems (under low water ratio condition, they can selective detection Al^{3+} by fluorescence "turn-on" response. While, under high water ratio and aggregate condition, they can selective detection Cu^{2+} trough AIE "turn off" pathway), while other **ADs** could not show any response to metal ions. In addition, test strips based on **AD10** has been prepared, which can conveniently detect Cu^{2+} in industrial wastewater. In summary, the structure-property relationships of simple azine derivatives on AIE and ions recognition performance were studied, which provided experience for future design of high efficiency and easy to make azine based fluorescence sensors.

Declaration of competing interest

The authors declare that there are no conflicts of interest.

Acknowledgments

This work was supported by the National Natural Science Foundation of China (NSFC, No. 22065031), the Key R & D Program of Gansu Province (No. 21YF5GA066), Gansu Province College Industry Support Plan Project (No. 2022CYZC-18), Natural Science Foundation of Gansu Province (Nos. 2020-0405-JCC-630, 20JR10RA088), Fundamental Research Funds for the Central Universities (Nos. 31920190041, 31920200002, 31920190018, 31920190013), Young Doctor Foundation of Gansu Province (No. 2021QB-148) and The Science and Technology Project Funded by Social Capital in Longnan City of Gansu Province (No. 2021-SZ-01).

Supplementary materials

Supplementary material associated with this article can be found, in the online version, at doi:10.1016/j.cclet.2022.107792.

References

[1] J. Mei, N.L.C. Leung, R.T.K. Kwok, J.W.Y. Lam, B.Z. Tang, Chem. Rev. 115 (2015) 11718–11940.
[2] Z.H. Zhang, Y.M. Zhang, T.B. Wei, et al., Chin. Chem. Lett. 34 (2023) 107085.
[3] P. Wang, S.X. Cao, T. Yin, X.L. Ni, Chin. Chem. Lett. 32 (2021) 1679–1682.
[4] L. Zhang, Y.F. Wang, M. Li, Q.Y. Gao, C.F. Chen, Chin. Chem. Lett. 32 (2021) 740–744.
[5] H. Yao, Q. Zhou, Q. Lin, et al., Chin. Chem. Lett. 31 (2020) 1231–1234.
[6] W.Q. Feng, Q. Su, B.Z. Tang, et al., J. Org. Chem. 85 (2020) 158–167.
[7] J.B. Xiong, H.T. Feng, J.P. Sun, et al., J. Am. Chem. Soc. 138 (2016) 11469–11472.
[8] J.Y. Gong, P.F. Wei, B.Z. Tang, et al., Chin. Chem. Lett. 29 (2018) 1493–1496.
[9] P.F. Wei, J.X. Zhang, B.Z. Tang, et al., J. Am. Chem. Soc. 140 (2018) 1966–1975.
[10] W.B. Dai, Z.X. Cai, Y.P. Dong, et al., ACS Mater. Lett. 3 (2021) 1767–1777.
[11] J.L. Tong, K.X. Zhang, B.Z. Tang, et al., J. Mater. Chem. C 8 (2020) 996–1001.
[12] G. Kumar, K. Paul, V. Luxami, Sens. Actuator. B: Chem. 263 (2018) 585–593.
[13] L. Peng, Z.J. Zhou, A.J. Tong, et al., Dye. Pigm. 108 (2014) 24–31.
[14] W.X. Tang, Y. Xiang, A.J. Tong, J. Org. Chem. 74 (2009) 2163–2166.
[15] Y.Y Xu, X.G. Gao, J.C. Leng, J.Z. Fan, CrystEngComm 23 (2021) 3582–3593.
[16] X.B. Haung, L.B. Qian, H.Y. Wu, et al., J. Mater. Chem. C 6 (2018) 5075–5096.
[17] Y.Z. Liu, X.B. Haung, H.Y. Wu, et al., Mater. Chem. C 4 (2016) 2862–2870.
[18] D. Magde, R. Wong, P.G Seybold, Photochem Photobiol 75 (2002) 327–334.
[19] S. Tsuzuki, K. Honda, T. Uchimaru, M. Mikami, K. Tanabe, J. Am. Chem. Soc. 124 (2002) 104–112.
[20] T. Lu, F. Chen, Acta Phsy. Chim. Sin. 28 (2012) 1–18.
[21] B. Das, M. Dolai, A. Jana, et al., J. Phys. Chem. A 125 (2021) 1490–1504.
[22] H.R. Qin, J.B. Huang, H. Liang, J. Lu, ACS Appl. Mater. Interfaces 13 (2021) 5668–5677.